Quantification of polarization bowing in III-nitrides by off-axis electron holography and impact on the polarization controversy

Qianqian Lan [1,*] Michael Schnedler [1] Keyan Ji [1] Jean-François Carlin [2] Raphaël Butté [2] Nicolas Grandjean [2] Rafal E. Dunin-Borkowski [1] and Philipp Ebert [1]

[1] *Ernst Ruska Centrum (ER-C-1), Forschungszentrum Jülich GmbH, 52425 Jülich, Germany*

[2] *Institute of Physics, Ecole Polytechnique Fédérale de Lausanne, CH-1015 Lausanne, Switzerland*

(Received 5 November 2025; accepted 9 March 2026; published 3 April 2026)

Polarization engineering has played an important role in advancing III-nitride semiconductor devices over recent decades. However, the exact magnitude and orientation of polarization remain highly debated, as significant discrepancies persist among different theoretical approaches and experiments. Therefore, we combine off-axis electron holography with surface potential calibration and self-consistent electrostatic modeling to directly measure quantitatively polarization changes at $In_xGa_{1-x}N/GaN$ interfaces. The results reveal a pronounced nonlinear, cubic dependence of spontaneous polarization on indium composition responsible for theoretical overestimation of polarization changes. Moreover, we show that only a layered hexagonal reference phase, rather than the zinc-blende phase, provides an accurate description of the experimental bowing of spontaneous polarization and hence a consistent theoretical framework of polarization in group-III nitrides. These results reconcile experiment and theory and provide a reliable basis for polarization engineering in InGaN alloys.

DOI: 10.1103/4rsc-ysk8

I. INTRODUCTION

Wurtzite (WZ) structure group III-nitride semiconductors exhibit substantial polarization, enabling key functionalities such as two-dimensional carrier gases [1], polarization doping [2], and the quantum-confined Stark effect [3], but also limiting quantum well efficiency. Hence polarization engineering is essential for achieving high-performance group III-nitride devices, requiring precise quantification and understanding. Yet, the magnitude, orientation, and composition dependence of polarization remain controversial [4].

On the theoretical side, the effective spontaneous polarization (P_{spon}) is not an absolute quantity, but rather defined relative to a chosen reference structure [5]. Consistent comparison across different III–nitride compounds therefore requires a common reference with well-defined—ideally zero—formal polarization, independent of chemical composition [6]. To date, zinc-blende (ZB) and layered hexagonal (LH) structures have been employed as references. Both reference structures predict significant nonlinear dependencies (bowing) of P_{spon} on alloy composition [7–9], but opposite orientations and very different magnitudes [8,10–14], raising concerns about the suitability of the chosen reference(s) [6,8,12,14,15] and thus rendering theoretical predictions inconclusive.

On the experimental side, measurements of polarization changes at $In_xGa_{1-x}N/GaN$ and $Al_xGa_{1-x}N/GaN$ heterointerfaces exhibit significant variability (see Fig. 2 of Ref. [6]), likely reflecting differences in samples' qualities, measurement accuracy, and surface effects. Moreover, the experimentally measured values are systematically lower than those predicted theoretically [6,16]. These issues cast doubts on both the precision of experimental quantification of polarization and the adequacy of current theoretical models for capturing the composition dependence of polarization in WZ group III-nitrides.

Here, we resolve this controversy by quantitatively determining the composition dependence of P_{spon} in high quality $In_xGa_{1-x}N$ using off-axis electron holography in transmission electron microscope (TEM). We directly measure phase shifts across biaxially strained $In_xGa_{1-x}N/GaN$ interfaces and extract total polarization changes through surface potential calibration and self-consistent electrostatic simulations. Combining this with high-resolution strain analysis allows separation of the piezoelectric contribution (P_{piezo}), yielding the effective P_{spon}. We find that only a layered hexagonal reference with [0001] orientation consistently describes the experimental data. Furthermore, P_{spon} exhibits a strong nonlinearity: at low indium content ($x < 0.25$) the bowing follows a parabolic form, while the overall dependence requires a cubic function, producing an S-shaped trend. These results provide quantitative insight into the intrinsic polarization of $In_xGa_{1-x}N$, reconcile theoretical and experimental discrepancies, and refine the framework for polarization in group-III nitrides.

II. METHODS

As a model system we use a metal organic vapor phase epitaxy grown heterostructure consisting of four 45 nm $In_xGa_{1-x}N$/300 nm GaN pairs on low threading dislocation

*Contact author: q.lan@fz-juelich.de

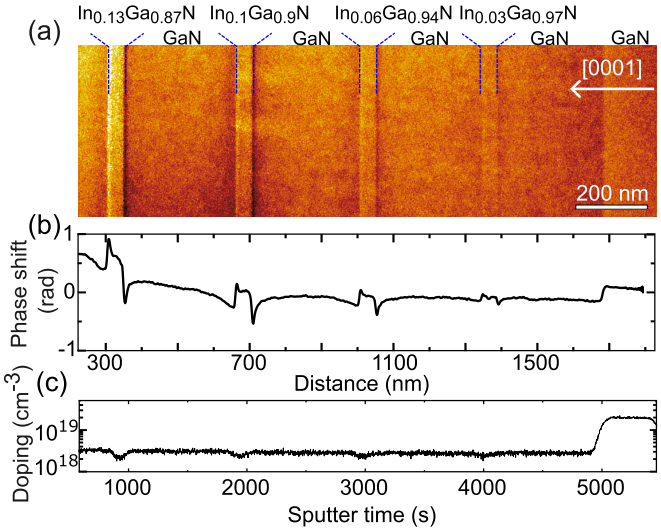

FIG. 1. (a) Electrostatic phase map of an $In_xGa_{1-x}N$ (45 nm)/GaN (300 nm) heterostructure with In composition x of 0.030, 0.062, 0.102, and 0.132 increasing from right to left. The [0001] growth direction points to the left side. (b) Optical electron phase profile extracted from the phase map shown in (a). (c) Si doping concentration measured by SIMS.

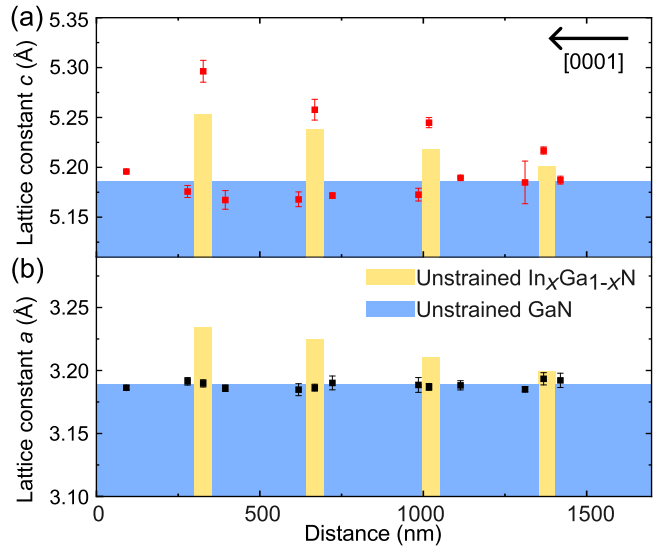

FIG. 2. (a) Out-of-plane c and (b) in-plane a lattice constants measured across the $GaN/In_xGa_{1-x}N/GaN$ heterostructure. The unstrained lattice constants of GaN and $In_xGa_{1-x}N$ calculated using Vegard's law are indicated by the blue and yellow histogram bars, respectively. The data (red and black symbols) reveal a lattice matched growth with biaxial strain.

density ($\sim 1 \times 10^6$ cm^{-2}) freestanding GaN(0001) substrate. X-ray diffraction yields In contents of the four layers of $x = 0.030 \pm 0.005$, 0.062 ± 0.005, 0.102 ± 0.005, and 0.132 ± 0.005. The Si doping level throughout the heterostructure is 3×10^{18} cm^{-3}($\pm$30%), while the GaN buffer includes an $n - n^+$ doping junction for surface potential calibration of TEM lamellae. The doping concentration, measured by time-of-flight secondary-ion mass spectrometry (TOF.SIMS 5, NCS IONTOF GmbH), is shown in Fig. 1(c).

Electron-transparent lamellae were prepared using a FEI Helios Nanolab 400s dual-beam focused ion beam (FIB) system using Ga ions at an acceleration voltage of 30 kV. To reduce surface damage and remove the amorphous layer induced during high-energy milling, low-voltage polishing steps at 5 kV and 2 kV were applied in the final stages of sample preparation. The crystalline thicknesses of the lamellas were determined via convergent beam electron diffraction (CBED). The thicknesses of the lamellas for EH were constant over the field of view.

The lattice constants and strain are derived from high angle annular dark field (HAADF) scanning TEM images by fitting Gaussians to the atomic columns, with the GaN buffer as calibration. The obtained strain values are in line with XRD measurement. The chemical composition is probed by energy dispersive x-ray spectroscopy (EDX). The EDX compositions are consistent with the secondary ion mass spectrometry (SIMS) results.

Off-axis electron holography measurements were carried out in a 300 kV image-aberration-corrected FEI Titan G2 60-300 HOLO microscope equipped with an electron biprism [17] using an electron beam dose of 17.8 e/(nm^{2}s). At this dose rate no changes of the phase contrast with beam exposure time occurred [18]. To suppress diffraction contrast and enhance the phase sensitivity, the lamellae were first tilted off-zone axis by 7.85° with the tilt axis perpendicular to the interface. Second, additional (perpendicular) tilts along an axis parallel to the interface normal were applied and hologram tilts series in steps of ~0.16° were acquired. The complex amplitude/phase images reconstructed from the hologram series were averaged for tilt ranges of ±(0.86–2.52)° during postprocessing, suppressing diffraction contrast, analogous to the precession in the four-dimensional scanning transmission electron microscopy (STEM) technique. Alternatively, some data points were extracted from holograms, where the tilts were adjusted such that the diffraction contrast is minimized. Both approached yield consistent data. The resolution of the phase maps obtained is 4.6 nm, on top of which a blurring due to tilt is present, yielding a combined resolution limit of about 7.5 nm.

III. EXPERIMENTAL RESULTS

Figure 1(a) shows an electrostatic phase map reconstructed from an electron hologram of the four $In_xGa_{1-x}N$ layers with increasing In composition x along the [0001] growth direction. The corresponding phase profile [Fig. 1(b)] reveals higher electron optical phase in each $In_xGa_{1-x}N$ layer relative to GaN, with the plateaus becoming more pronounced as In concentration increases. Beyond the plateaus, the profile exhibits asymmetric interface peaks: large positive peaks at $GaN/In_xGa_{1-x}N$ interfaces (left side) and negative peaks at $In_xGa_{1-x}N/GaN$ interfaces (right side), an asymmetry that grows with indium content.

In addition, the strain state was assessed from a and c lattice constants measured by atomically resolved HAADF imaging (Fig. 2). GaN layers show bulk-like lattice constants and thus are nearly unstrained, while $In_xGa_{1-x}N$ layers

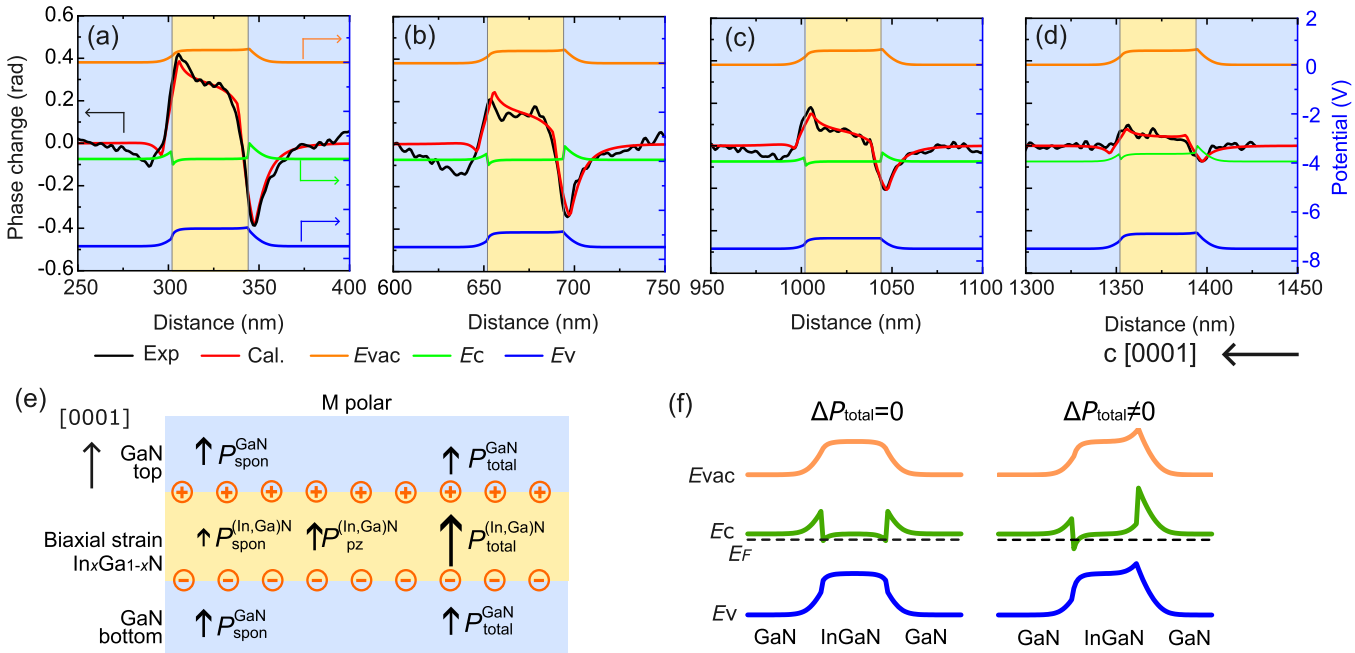

FIG. 3. (a)–(d) Experimental (black) and its best-fit calculated (red line) phase shift profiles, the potential of vacuum (orange), conduction band (green), and valence band (blue) across the interface of GaN/$In_xGa_{1-x}N$/GaN heterostructures with In composition x of 0.030, 0.062, 0.102, and 0.132, respectively. The particular lamella had a thickness of 137 nm. (e) Sketch map of spontaneous polarization, piezoelectric polarization, interface polarization difference, and bound charges in the heterostructures as deduced in the main text. (f) Band diagrams of the heterostructure (left) without polarization and (right) with polarization.

exhibit a lattice constants matching GaN and enlarged c lattice constants, consistent with biaxially strained growth.

IV. QUANTITATIVE DETERMINATION OF POLARIZATION

For quantitative analysis, zoomed phase profiles of each $In_xGa_{1-x}N$ layer are shown as black lines in Figs. 3(a)–3(d). The plateau regions mainly arise from differences in mean inner potential and electron affinity between $In_xGa_{1-x}N$ and GaN [19]. In contrast, the asymmetric positive and negative peaks indicate bound charges at heterointerfaces due to polarization discontinuities [cf. Fig. 3(f)]. Their extent and slope are shaped by electrostatic screening from free carriers. Note, in commonly used (undoped) quantum wells the polarization field is unscreened and thus linear [20–22]. The $In_xGa_{1-x}N$ layers used here are thick enough to screen most of the polarization field in the center of the layers, leading to separate peaks. Thus the holography-derived electrostatic potential reflects a complex interplay of mean inner potential and the free carrier redistribution caused, e.g., by electron affinity, polarization, and electrostatic screening. Additionally, FIB-induced defects create surface potentials at lamella surfaces [23,24]. To disentangle these effects and quantify polarization changes, we employ self-consistent electrostatic simulations fitted to the data.

The simulation follows a three-step approach [19]: (i) determine the TEM lamella surface potential using a grown-in doping structure [19,24], (ii) calculate self-consistently the electrostatic potential and carrier concentrations of chemically sharp interfaces including polarization and surface potential using a finite-difference Poisson solver assuming Fermi-Dirac carrier statistics [25,26], and (iii) compute the electron optical phase map by integrating the potential along the beam direction [19]. The calculated profiles, broadened by a moving average to account for experimental tilt, are fitted to the data with polarization differences between GaN and $In_xGa_{1-x}N$ as free parameter.

A. Determination of surface potentials

To quantitatively extract polarization changes at $In_xGa_{1-x}N$/GaN interfaces, calibration of the lamella surface potential is required. FIB preparation induces an amorphous shell and a defect-rich crystalline zone, leading to Fermi-level pinning and carrier depletion near the surfaces [19,23,24,27,28]. These depletion regions reduce the electrically active thickness of the lamella, such that neglecting them would misestimate the polarization discontinuity.

The calibration follows Refs. [19,23,24,29], using the n^+-n doping step in the GaN buffer. At this step a phase shift of 0.22 ± 0.02 rad is measured [Fig. 1(b)]. Based on the doping concentrations [Fig. 1(c)], electrostatic simulations yield a surface Fermi-level pinning of 0.69 ± 0.10 eV above the valence band edge, consistent with earlier work [19,23]. The pinning originates from C_N implanted during FIB preparation of the TEM lamellae [23,29]. The pinning is defined by the $(-/0)$ charge-transfer level of C_N, whose energy relative to the vacuum energy is almost identical for both InN and GaN [30]. Thus the extracted pinning level can be used uniformly across all layers as a calibrated input for the phase analysis.

TABLE I. Fit values of the mean inner potential differences with respect to GaN for the different $In_xGa_{1-x}N$ layers.

x	$MIP_{In_xGa_{1-x}N}$-MIP_{GaN} (V)
0.030	0.27 ± 0.06
0.062	0.40 ± 0.08
0.102	0.56 ± 0.12
0.132	0.74 ± 0.14

B. Mean inner potential differences

As outlined above, the differences in mean inner potential between the GaN and $In_xGa_{1-x}N$ layers induce the plateau offsets between the materials in the phase profiles. Hence the mean inner potential differences are used as fit parameter. The obtained values are given in Table I. Note that the polarization induced features at the interfaces are not affected by the mean inner potential differences and hence essentially no cross-correlation of the errors is present.

C. Extraction of polarization from phase profiles

The total polarization change $\Delta P_{\text{total}} = P_{\text{total}}^{\text{GaN}} - P_{\text{total}}^{\text{(In,Ga)N}}$ at the interface of (In,Ga)N grown on top of GaN is obtained by fitting simulated to experimental phase profiles. Figures 3(a)–3(d) show excellent agreement between experiments (black) and simulations (red) for all four layers.

The corresponding simulated band diagrams, also shown in Figs. 3(a)–3(d) as orange, green, and blue lines, reveal pronounced band bending at the interfaces due to bound charges originating from polarization discontinuities: negative charges at $In_xGa_{1-x}N$/GaN(0001) and positive ones at GaN/$In_xGa_{1-x}N$(0001) interfaces. Figure 3(f) highlights the effect of polarization by comparing calculations without ($\Delta P_{\text{total}} = 0$, left) and with finite ΔP_{total} (right). Without polarization, the band profile remains nearly symmetric and dominated by electron affinity and band gap offsets. Including polarization introduces a screened electric field, giving rise to an overall asymmetric band structure. At the GaN/$In_xGa_{1-x}N$ interface, the positive bound charge induces a 2DEG, efficiently screening the polarization field. To avoid inaccuracies from neglecting quantized states at the interfaces in our purely electrostatic model (without solutions of the Schrödinger equation), ΔP_{total} is extracted at the $In_xGa_{1-x}N$/GaN interface with negative bound charge, where no 2DEG forms.

The obtained polarization is consistently larger in the $In_xGa_{1-x}N$ layers than in GaN, resulting in negative polarization changes ΔP_{total} as defined above. The obtained ΔP_{total} values derived from three lamellae are shown in Fig. 4 as red circles. We obtained a weighted average of the polarization change $\Delta P_{\text{total}}^{\text{avg,expt}} = -0.00091 \pm 0.00034$, -0.00442 ± 0.00107, -0.00622 ± 0.00089, and -0.0077 ± 0.00135 C/m^2 for $x = 0.03$, 0.062, 0.102, and 0.132, respectively (Fig. 4). These values demonstrate both reproducibility and a clear compositional trend. The analysis assumes polarization along [0001], consistent with the LH reference model of Dreyer *et al.* [6]. If the polarization orientation is reversed (as in a ZB reference model), the ΔP_{total} values simply switch sign while retaining the same magnitudes.

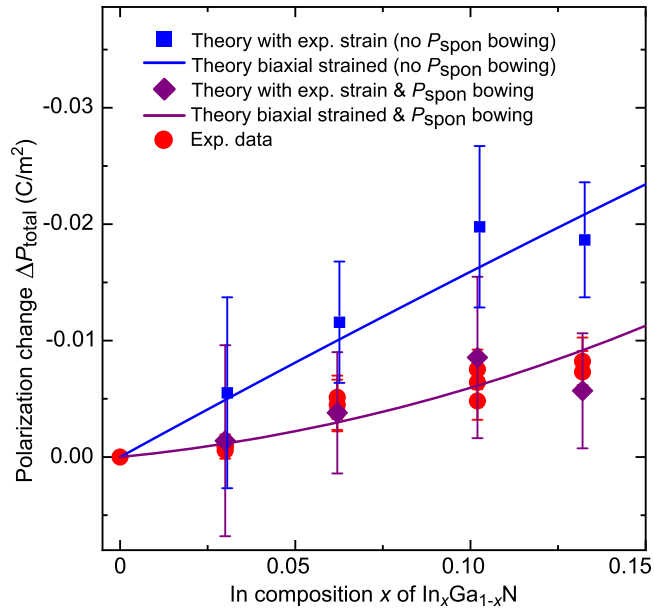

FIG. 4. Polarization change, $\Delta P_{\text{total}} = P_{\text{total}}^{\text{GaN}} - P_{\text{total}}^{\text{(In,Ga)N}}$, at the biaxially strained $In_xGa_{1-x}N$/GaN interface as a function of In composition x. Red circles represent values extracted from electron holography in this work. Their error bars originate from the noise of the phase profiles and the assumed 30% error of Si doping. The blue solid line represents the prediction of Eqs. (1) and (2) for an ideally biaxially strained $In_xGa_{1-x}N$/GaN interface without bowing of the spontaneous polarization [6]. In contrast, the purple solid line shows the theory including the here determined bowing of the spontaneous polarization for an ideally biaxially strained $In_xGa_{1-x}N$/GaN interface. The blue solid squares and purple solid diamonds represent the same, i.e., theory without and with bowing of the spontaneous polarization, respectively, but using the experimentally measured strain values. The error bars primarily stem from the accuracy of the lattice constant measurement.

V. DISCUSSION OF POLARIZATION CHANGES

A. Comparison with previous measurements

The polarization changes at the biaxially strained $In_xGa_{1-x}N$/GaN interface from our electron holography measurements (red circles) align well with the range of previous data (see compilation in Ref. [6]).

B. Comparison with the modern theory of polarization

Next, we compare our experimental results with predictions of the modern theory of polarization [5] in wurtzite group-III nitrides. For a biaxially strained $In_xGa_{1-x}N$/GaN interface, a strain-free theory is inapplicable (predicting positive polarization changes, contrary to experiment). We therefore recall the strain-dependent model for the total polarization along the c direction [6]:

$$P_{\text{total}} = P_{\text{spon}} + 2\epsilon_1(e_{31} - P_{\text{spon}}) + \epsilon_3 e_{33}, \tag{1}$$

with, in the case of ideal biaxial strain,

$$\epsilon_3 = -2\frac{C_{13}}{C_{33}}\epsilon_1, \tag{2}$$

TABLE II. Materials constants used here for GaN and InN. The piezoelectric constants are the average of values compiled in Tables 2 and 3 of Ref. [31] and those reported in Refs. [6,32–34] with standard error of the mean. The effective spontaneous polarizations with ZB reference structure $P_{\text{spon, ZB}}$ are taken from Ref. [6]. The respective values with LH reference structure $P_{\text{spon, LH}}$ are taken from Ref. [8], since this work calculated $P_{\text{spon, LH}}$ also for ternary compounds, needed for comparison with experimental values in Fig. 6. The $P_{\text{spon, LH}}$ values for the binary GaN and InN compounds are almost identical to those of Ref. [6]. The elastic constants are the average of values given in [34–44] with the standard error of the mean.

	GaN	InN
e_{31} (C/m^2)	-0.408 ± 0.028	-0.501 ± 0.026
e_{33} (C/m^2)	0.768 ± 0.047	0.934 ± 0.059
$P_{\text{spon, LH}}$ (C/m^2)	1.299	1.032
$P_{\text{spon, ZB}}$ (C/m^2)	-0.035	-0.053
C_{13} (GPa)	108.2 ± 2.2	95.2 ± 2.3
C_{33} (GPa)	391.9 ± 3.3	231.9 ± 3.8

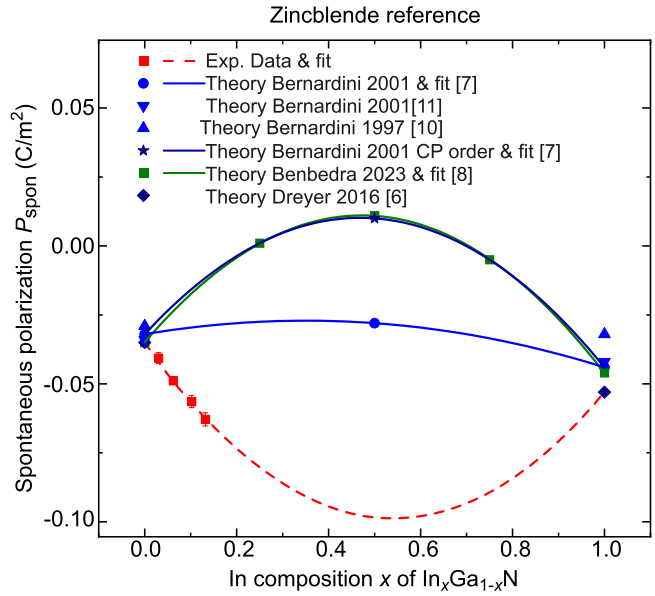

FIG. 5. Composition dependence of the spontaneous polarization P_{spon} of $\text{In}_x\text{Ga}_{1-x}\text{N}$ derived using spontaneous polarization values with ZB reference structure. The red squares show the values determined from electron holography measurements, while the navy diamonds, olive squares, and blue colored symbols and navy star represent calculated values from Refs. [6–8,10,11]. The theoretical results do not match to the sign of curvature of experimental data, suggesting that the ZB reference structure is inadequate to describe the experimentally determined composition dependence of the effective spontaneous polarization.

where P_{spon} is the effective spontaneous polarization. $e_{3\text{i}}$ are the proper piezoelectric constants and C_{13} and C_{33} are the elastic constants. For improving the accuracy of these constants we took an average of the literature values for WZ structure GaN and InN, as summarized in Table II. ϵ_{i} is the strain in the a-b (0001) plane ($i = 1$) and [0001] c direction ($i = 3$).

As a first approximation, the expected polarization change ΔP_{total} for an ideally biaxially strained interface, computed from Eqs. (1) and (2) using linear interpolation (Vegard's law) of P_{spon}, e_{3i}, and C_{ij}, is shown in Fig. 4 as a blue line. Here, the LH reference structure is used; the ZB reference gives nearly identical values [6]. Alternatively the strain values can be derived directly from the measured a and c lattice constants (Fig. 2) without using Eq. (2) shown as blue squares. For both the ideal biaxial and measured strain, the polarization changes calculated using Eq. (1) exceed our experimental as well as most literature values.

This suggests that either some material constants used in Eqs. (1) and (2) are inaccurate or their linear interpolation is insufficient due to bowing. Three types of parameters are relevant.

(i) Elastic constants. Their effect is minor because ϵ_3 contributes little to polarization, making bowing-induced deviations negligible. Density functional theory (DFT) predicts a linear composition dependence for (Al,Ga)N and (In,Al)N [45], implying a similar behavior for (In,Ga)N. This is supported by the fact that using measured strain values (instead of elastic constants) Eq. (1) still overestimates polarization changes. Elastic constants are therefore not critical.

(ii) Piezoelectric constants. Bowing can also be neglected since (a) the difference between GaN and the largest In composition here is below 3%, (b) DFT predicts a linear composition dependence of the piezoelectric constants of (Al,Ga)N and (In,Al)N (Figs. 26 and 27 in [45]), suggesting the same for (In,Ga)N, and (c) DFT predicts a nearly linear composition dependence of the piezoelectric polarization for (In,Ga)N [8].

Using smaller piezoelectric constants would reduce polarization changes in Eq. (1), but matching experiments would require a 60% reduction, corresponding to a deviation from literature values of $\sim 8\sigma$ (Table II), which is extremely unlikely. Thus deviations cannot be attributed to piezoelectric constants.

(iii) Effective spontaneous polarization. For (In,Ga)N alloys only two DFT calculations address the composition dependence of the spontaneous polarization [7,8], while all others restrict the calculations to the binary end members [6,10,11,46]. Taking ternary compositions into account, DFT shows significant bowing in the composition dependence of spontaneous polarization [7,8].

Therefore, we used the effective spontaneous polarization $P_{\text{spon}}(x)$ in Eq. (1) as a fit parameter to fit the experimental weighted average polarization change $\Delta P_{\text{total}}^{\text{avg,expt}}(x)$ (given above), using the measured strains and constants given in Table II. The analysis is performed for two reference cases: (i) polarization pointing along the [000$\bar{1}$] ($-c$ direction), using $P_{\text{spon,ZB}}$ values with ZB reference structure), and (ii) polarization pointing along the [0001] ($+c$ direction), using $P_{\text{spon,LH}}$ with the LH reference structure. The extracted P_{spon} values for $\text{In}_x\text{Ga}_{1-x}\text{N}$ are plotted as red squares in Figs. 5 and 6 for ZB and LH reference structures, respectively. Error bars reflect a 0.5% uncertainty in In composition and strain measurement errors.

Calculated P_{spon} values are also displayed for comparison as blue/green symbols. With the ZB reference structure, the

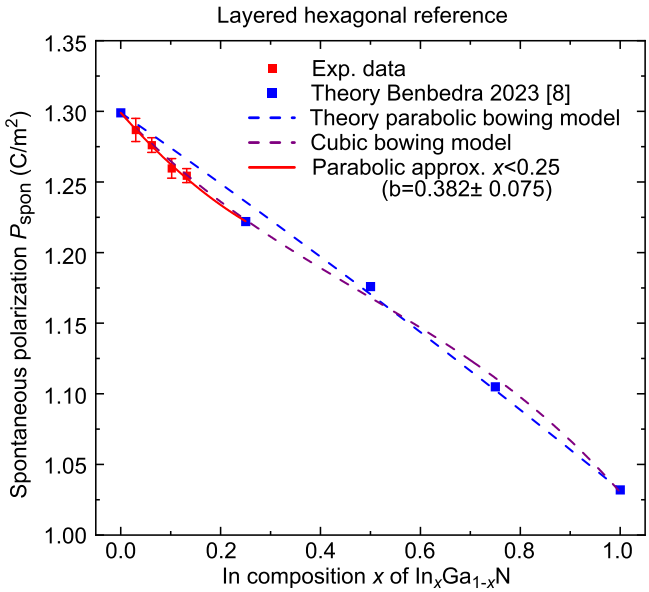

FIG. 6. Composition dependence of the spontaneous polarization P_{spon} of $In_xGa_{1-x}N$ derived using spontaneous polarization values with LH reference structure. The red squares show the values determined from electron holography measurements while the blue squares represent calculated values from Ref. [8]. The data points deviate from Vegard's law. The cubic fit to all calculated and measured data points (purple dashed line) reveals that even a parabolic bowing (blue dashed line) cannot describe the whole composition range. Only for low In concentration, $x < 0.25$, is a parabolic fit (red line) accurate, yielding a bowing parameter of 0.382 ± 0.075 C/m^2.

calculated bowing shows a negative curvature, failing to capture the experimentally found positive curvature (Fig. 5). In contrast, the P_{spon} values based on the LH reference structure agree well with calculations (Fig. 6), indicating that only the LH-based polarization model [6,8] accurately describes the experimental data. This supports effective spontaneous as well as total polarization pointing in the [000+1] direction, as sketched in Fig. 3(e). This orientation is consistent with high-resolution TEM imaging of group-III and N column displacements [4,13]. Therefore, subequent discussion focuses on the LH-based P_{spon} values in Fig. 6.

We now address the optimal bowing model. The parabolic fit (blue dashed line in Fig. 6) based solely on calculated $P_{spon}(x)$ values (blue symbols) [8] does not match the experimental data (red symbols). Instead, a better description incorporating both experimental and calculated values requires a cubic (S-shaped) composition dependence, with the best fit (purple dashed line) given in units of C/m^2 by

$$P_{spon}(x) = 1.299(1-x) + 1.0303x - b(x)\cdot x(1-x), \quad (3)$$

where

$$b(x) = 0.105 - 0.238x. \quad (4)$$

However, since experimental data are currently limited to the Ga-rich side of (In,Ga)N, we adopt a more practical parabolic fit valid for small In contents ($x < 0.25$) in units of C/m^2, shown as the red line:

$$P_{spon}(x) = 1.299(1-x) + 1.278x - 0.382x(1-x) \quad \text{with } x < 0.25. \quad (5)$$

The full composition dependence of $P_{spon}(x)$ will require revision as data for In-rich alloys become available.

Next, we compare the total polarization change, $\Delta P_{total}(x)$, calculated using the refined bowing parameters for $P_{spon}(x)$ at $x < 0.25$ [Eq. (5)], with experimental values in Fig. 4. The computed $\Delta P_{total}(x)$ (purple diamonds) shows significantly improved agreement with the measured data (red circles) compared to the model without spontaneous polarization bowing (blue line and symbols). This confirms that bowing is a key factor in resolving discrepancies between experiment and theory.

Finally, the strain values were calculated assuming a linear interpolation of the lattice constants, due to inconclusive literature values [47–50]. If a lattice constant bowing would be considered, the spontaneous polarization would still remain smaller than the linear interpolation, corroborating the results.

VI. CONCLUSION

Using off-axis electron holography combined with surface potential calibration and self-consistent electrostatic modeling, we quantitatively determined the total polarization change at $In_xGa_{1-x}N$/GaN interfaces. By measuring the strain in STEM images, we separated the total polarization change into its piezoelectric and spontaneous components. The effective spontaneous polarization exhibits a pronounced nonlinear composition dependence: at low indium concentrations it can be described by a parabolic form, while over the full composition range a cubic dependence is required. Fitting the experimental data for $x < 0.25$ yields a bowing parameter of 0.382 ± 0.075 C/m^2. This bowing of the spontaneous polarization explains the systematic overestimation of total polarization changes in theoretical models. Furthermore, we find that only a layered hexagonal reference phase provides an accurate description of the experimentally determined bowing of the spontaneous polarization, in contrast to the commonly used zinc-blende reference. These results establish a consistent theoretical framework for group-III nitrides and clarify the composition dependence of polarization in the technologically important $In_xGa_{1-x}N$ alloy.

ACKNOWLEDGMENTS

The authors thank L. Risters and Y. Lu for FIB preparation of some of the TEM lamellae and H. Eisele for fruitful discussions. The authors gratefully acknowledge the use of resources in the "ER-C 2.0" National Research Infrastructure for High-Resolution Electron Microscopy in Forschungszentrum Jülich GmbH.

DATA AVAILABILITY

The data that support the findings of this article are not publicly available. The data are available from the authors upon reasonable request.

[1] R. Chaudhuri, S. J. Bader, Z. Chen, D. A. Muller, H. G. Xing, and D. Jena, A polarization-induced 2D hole gas in undoped gallium nitride quantum wells, Science **365**, 1454 (2019).

[2] J. Simon, V. Protasenko, C. Lian, H. Xing, and D. Jena, Polarization-induced hole doping in wide–band-gap uniaxial semiconductor heterostructures, Science **327**, 60 (2010).

[3] T. Takeuchi, S. Sota, M. Katsuragawa, M. Komori, H. Takeuchi, H. Amano, and I. Akasaki, Quantum-confined stark effect due to piezoelectric fields in gainn strained quantum wells, Jpn. J. Appl. Phys. **36**, L382 (1997).

[4] H. Ye, P. Wang, R. Wang, J. Wang, X. Xu, R. Feng, T. Wang, W.-Y. Tong, F. Liu, B. Sheng, W. Ma, B. An, H. Li, Z. Chen, C.-G. Duan, W. Ge, B. Shen, and X. Wang, Experimental determination of giant polarization in wurtzite III-nitride semiconductors, Nat. Commun. **16**, 3863 (2025).

[5] R. Resta and D. Vanderbilt, Theory of polarization: A modern approach, in *Physics of Ferroelectrics: A Modern Perspective* (Springer, Berlin, Heidelberg, 2007), pp. 31–68.

[6] C. E. Dreyer, A. Janotti, C. G. Van de Walle, and D. Vanderbilt, Correct implementation of polarization constants in wurtzite materials and impact on III-nitrides, Phys. Rev. X **6**, 021038 (2016).

[7] F. Bernardini and V. Fiorentini, Nonlinear macroscopic polarization in III-V nitride alloys, Phys. Rev. B **64**, 085207 (2001).

[8] A. Benbedra, S. Meskine, A. Boukortt, H. Abbassa, and E. H. Abbes, Polarization properties of wurtzite III-nitride alloys using the hexagonal reference structure, ECS J. Sol. State Sci. Technol. **12**, 103008 (2023).

[9] H. Wang, N. Adamski, S. Mu, and C. G. Van de Walle, Piezoelectric effect and polarization switching in $Al_{1-x}Sc_xN$, J. Appl. Phys. **130**, 104101 (2021).

[10] F. Bernardini, V. Fiorentini, and D. Vanderbilt, Spontaneous polarization and piezoelectric constants of III-V nitrides, Phys. Rev. B **56**, R10024 (1997).

[11] F. Bernardini, V. Fiorentini, and D. Vanderbilt, Accurate calculation of polarization-related quantities in semiconductors, Phys. Rev. B **63**, 193201 (2001).

[12] A. Ahmad, P. Strak, K. Koronski, P. Kempisty, K. Sakowski, J. Piechota, I. Grzegory, A. Wierzbicka, S. Kryvyi, E. Monroy, A. Kaminska, and S. Krukowski, Critical evaluation of various spontaneous polarization models and induced electric fields in III-nitride multi-quantum wells, Materials **14**, 4935 (2021).

[13] S. Fichtner, M. Yassine, C. G. Van de Walle, and O. Ambacher, Clarification of the spontaneous polarization direction in crystals with wurtzite structure, Appl. Phys. Lett. **125**, 040501 (2024).

[14] P. Strak, P. Kempisty, K. Sakowski, J. Piechota, I. Grzegory, E. Monroy, A. Kaminska, and S. Krukowski, Spontaneous and piezo polarization versus polar surfaces: Fundamentals and *ab initio* calculations, Materials **18**, 1489 (2025).

[15] J. Cañas, M. Yassine, and O. Ambacher, Giant spontaneous polarization in zinc-blende III-V semiconductors, Phys. Rev. B **112**, L081201 (2025).

[16] V. Fiorentini, F. Bernardini, and O. Ambacher, Evidence for nonlinear macroscopic polarization in III–V nitride alloy heterostructures, Appl. Phys. Lett. **80**, 1204 (2002).

[17] A. Kovács, R. Schierholz, and K. Tillmann, FEI Titan G2 80-200 CREWLEY, JLSRF **2**, A43 (2016).

[18] K. Ji, Quantitative investigation of point defects and their dynamics in focused ion beam-prepared group III-nitride lamellas by off-axis electron holography, Ph.D. thesis, RWTH Aachen University, 2024.

[19] Y. Wang, M. Schnedler, Q. Lan, F. Zheng, L. Freter, Y. Lu, U. Breuer, H. Eisele, J.-F. Carlin, R. Butté, N. Grandjean, R. E. Dunin-Borkowski, and P. Ebert, Interplay of anomalous strain relaxation and minimization of polarization changes at nitride semiconductor heterointerfaces, Phys. Rev. B **102**, 245304 (2020).

[20] D. Cherns, J. Barnard, and F. Ponce, Measurement of the piezoelectric field across strained InGaN/GaN layers by electron holography, Solid State Commun. **111**, 281 (1999).

[21] V. Boureau and D. Cooper, Highly spatially resolved mapping of the piezoelectric potentials in InGaN quantum well structures by off-axis electron holography, J. Appl. Phys. **128**, 155704 (2020).

[22] D. Cooper, V. Boureau, A. Even, F. Barbier, and A. Dussaigne, Determination of the internal piezoelectric potentials and indium concentration in InGaN based quantum wells grown on relaxed InGaN pseudo-substrates by off-axis electron holography, Nanotechnology **31**, 475705 (2020).

[23] K. Ji, M. Schnedler, Q. Lan, F. Zheng, Y. Wang, Y. Lu, H. Eisele, J.-F. Carlin, R. Butté, N. Grandjean, R. E. Dunin-Borkowski, and Ph. Ebert, Identification and thermal healing of focused ion beam-induced defects in GaN using off-axis electron holography, Appl. Phys. Express **17**, 016505 (2024).

[24] K. Ji, M. Schnedler, Q. Lan, J.-F. Carlin, R. Butté, N. Grandjean, R. Dunin-Borkowski, and P. Ebert, Origin of giant enhancement of phase contrast in electron holography of modulation-doped n-type GaN, Ultramicroscopy **264**, 114006 (2024).

[25] M. Schnedler, V. Portz, P. H. Weidlich, R. E. Dunin-Borkowski, and Ph. Ebert, Quantitative description of photoexcited scanning tunneling spectroscopy and its application to the GaAs(110) surface, Phys. Rev. B **91**, 235305 (2015).

[26] M. Schnedler, R. E. Dunin-Borkowski, and Ph. Ebert, Importance of quantum correction for the quantitative simulation of photoexcited scanning tunneling spectra of semiconductor surfaces, Phys. Rev. B **93**, 195444 (2016).

[27] M. Beleggia, P. F. Fazzini, P. G. Merli, and G. Pozzi, Influence of charged oxide layers on TEM imaging of reverse-biased $p-n$ junctions, Phys. Rev. B **67**, 045328 (2003).

[28] D. Wolf, A. Lubk, A. Lenk, S. Sturm, and H. Lichte, Tomographic investigation of fermi level pinning at focused ion beam milled semiconductor surfaces, Appl. Phys. Lett. **103**, 264104 (2013).

[29] K. Ji, M. Schnedler, Q. Lan, J.-F. Carlin, R. Butté, N. Grandjean, R. E. Dunin-Borkowski, and Ph. Ebert, Quantifying carbon site switching dynamics in GaN by electron holography, Phys. Rev. Res. **7**, 013200 (2025).

[30] J. L. Lyons, A. Janotti, and C. G. Van de Walle, Effects of carbon on the electrical and optical properties of InN, GaN, and AlN, Phys. Rev. B **89**, 035204 (2014).

[31] M. Feneberg and K. Thonke, Polarization fields of III-nitrides grown in different crystal orientations, J. Phys.: Condens. Matter **19**, 403201 (2007).

[32] K. Shimada, First-principles determination of piezoelectric stress and strain constants of wurtzite III–V nitrides, Jpn. J. Appl. Phys. **45**, L358 (2006).

[33] K. Adachi, H. Ogi, A. Nagakubo, N. Nakamura, M. Hirao, M. Imade, M. Yoshimura, and Y. Mori, Piezoelectric coefficients of

GaN determined by hopping conduction of carriers, Appl. Phys. Lett. **109**, 182108 (2016).

[34] X.-P. Shen, J.-B. Lin, R.-Y. Hu, Y.-C. Liu, L.-Q. Xu, H.-B. Niu, X.-F. Xiao, and V. Wang, Compositional effects on structural, electronic, elastic, piezoelectric and dielectric properties of gainn alloys: a first-principles study, RSC Adv. **14**, 6752 (2024).

[35] A. Polian, M. Grimsditch, and I. Grzegory, Elastic constants of gallium nitride, J. Appl. Phys. **79**, 3343 (1996).

[36] K. Kim, W. R. L. Lambrecht, and B. Segall, Erratum: Elastic constants and related properties of tetrahedrally bonded BN, AlN, GaN, and InN [Phys. Rev. B 53, 16310 (1996)], Phys. Rev. B **56**, 7018(E) (1997).

[37] K. Shimada, T. Sota, and K. Suzuki, First-principles study on electronic and elastic properties of BN, AlN, and GaN, J. Appl. Phys. **84**, 4951 (1998).

[38] C. Deger, E. Born, H. Angerer, O. Ambacher, M. Stutzmann, J. Hornsteiner, E. Riha, and G. Fischerauer, Sound velocity of $Al_xGa_{1-x}N$ thin films obtained by surface acoustic-wave measurements, Appl. Phys. Lett. **72**, 2400 (1998).

[39] N. Aïchoune, V. Potin, P. Ruterana, A. Hairie, G. Nouet, and E. Paumier, An empirical potential for the calculation of the atomic structure of extended defects in wurtzite GaN, Comput. Mater. Sci. **17**, 380 (2000).

[40] J.-M. Wagner and F. Bechstedt, Properties of strained wurtzite GaN and AlN: *Ab initio* studies, Phys. Rev. B **66**, 115202 (2002).

[41] S. P. Łepkowski, J. A. Majewski, and G. Jurczak, Nonlinear elasticity in III-N compounds: *Ab initio* calculations, Phys. Rev. B **72**, 245201 (2005).

[42] F. Morales, D. González, J. Lozano, R. García, S. Hauguth-Frank, V. Lebedev, V. Cimalla, and O. Ambacher, Determination of the composition of $In_xGa_{1-x}N$ from strain measurements, Acta Mater. **57**, 5681 (2009).

[43] K. Sarasamak, S. Limpijumnong, and W. R. L. Lambrecht, Pressure-dependent elastic constants and sound velocities of wurtzite SiC, GaN, InN, ZnO, and CdSe, and their relation to the high-pressure phase transition: A first-principles study, Phys. Rev. B **82**, 035201 (2010).

[44] M.-M. Soumelidou, I. Belabbas, J. Kioseoglou, P. Komninou, J. Chen, and T. Karakostas, Strain and elastic constants of GaN and InN, Comput. Condens. Matter **10**, 25 (2017).

[45] O. Ambacher, B. Christian, N. Feil, D. F. Urban, C. Elsässer, M. Prescher, and L. Kirste, Wurtzite ScAlN, InAlN, and GaAlN crystals, a comparison of structural, elastic, dielectric, and piezoelectric properties, J. Appl. Phys. **130**, 045102 (2021).

[46] P. Strak, P. Kempisty, K. Sakowski, A. Kaminska, D. Jankowski, K. P. Korona, K. Sobczak, J. Borysiuk, M. Beeler, E. Grzanka, E. Monroy, and S. Krukowski, *Ab initio* and experimental studies of polarization and polarization related fields in nitrides and nitride structures, AIP Adv. **7**, 015027 (2017).

[47] Y. Cui, S. Lee, C. Freysoldt, and J. Neugebauer, Role of biaxial strain and microscopic ordering for structural and electronic properties of $In_xGa_{1-x}N$, Phys. Rev. B **92**, 085204 (2015).

[48] Y.-C. Tsai and C. Bayram, Structural and electronic properties of hexagonal and cubic phase AlGaInN alloys investigated using first principles calculations, Sci. Rep. **9**, 6583 (2019).

[49] Z. Dridi, B. Bouhafs, and P. Ruterana, First-principles investigation of lattice constants and bowing parameters in wurtzite $Al_xGa_{1-x}N$, $In_xGa_{1-x}N$ and $In_xAl_{1-x}N$ alloys, Semicond. Sci. Technol. **18**, 850 (2003).

[50] B.-T. Liou, C.-Y. Lin, S.-H. Yen, and Y.-K. Kuo, First-principles calculation for bowing parameter of wurtzite $In_xGa_{1-x}N$, Opt. Commun. **249**, 217 (2005).